



**HAL**  
open science

# Yield design-based numerical analysis of three-dimensional reinforced concrete structures

Hugues Vincent, Mathieu Arquier, Jeremy Bleyer, Patrick de Buhan

► **To cite this version:**

Hugues Vincent, Mathieu Arquier, Jeremy Bleyer, Patrick de Buhan. Yield design-based numerical analysis of three-dimensional reinforced concrete structures. *International Journal for Numerical and Analytical Methods in Geomechanics*, 2018, 42 (18), pp.2177-2192. 10.1002/nag.2850 . hal-01855342

**HAL Id: hal-01855342**

**<https://enpc.hal.science/hal-01855342>**

Submitted on 7 Aug 2018

**HAL** is a multi-disciplinary open access archive for the deposit and dissemination of scientific research documents, whether they are published or not. The documents may come from teaching and research institutions in France or abroad, or from public or private research centers.

L'archive ouverte pluridisciplinaire **HAL**, est destinée au dépôt et à la diffusion de documents scientifiques de niveau recherche, publiés ou non, émanant des établissements d'enseignement et de recherche français ou étrangers, des laboratoires publics ou privés.

# **YIELD DESIGN BASED NUMERICAL ANALYSIS OF THREE-DIMENSIONAL REINFORCED CONCRETE STRUCTURES**

H. Vincent<sup>1,2</sup>, M. Arquier<sup>1</sup>, J. Bleyer<sup>2</sup>, P. de Buhan<sup>2</sup>

<sup>1</sup>Strains, Paris, France

<sup>2</sup>Laboratoire Navier, UMR 8205, Ecole des Ponts ParisTech, IFSTTAR, CNRS, UPE, Champs-sur-Marne, France

## **ABSTRACT**

The objective of this contribution is to present some new recent developments regarding the evaluation of the ultimate bearing capacity of massive three-dimensional reinforced concrete structures which cannot be modelled as 1D (beams) or 2D (plates) structural members. The approach is based upon the implementation of the lower bound static approach of yield design through a discretization of the three-dimensional structure into tetrahedral finite elements, on the one hand, the formulation of the corresponding optimization problem in the context of Semi-definite Programming (SDP) techniques, on the other hand. Another key feature of the method lies in the treatment of the concrete-embedded reinforcing bars not as individual elements, but by resorting to an extension of the yield design homogenization approach. The whole procedure is first validated on the rather simple illustrative problem of a uniformly loaded simply supported beam, then applied to the design of a bridge pier cap taken as an example of more complex and realistic structure.

**Keywords:** reinforced concrete structures, yield design, semi-definite programming, homogenization.

## 1. INTRODUCTION

The yield design [1] or limit analysis [2] approach provides a suitable theoretical as well as computational framework for the *Ultimate Limit State Design* of structures in general and reinforced concrete structures in particular. In the situation when the structure is made of an assemblage of 1D (beams or arches) or 2D (plates or shells) structural members, its ultimate bearing capacity may be evaluated from a previously determined interaction yield criterion involving generalized stresses such as axial-membrane forces and bending moments. This method, which proves particularly attractive from an engineering point of view, has been quite recently used for spatial frame structures [3] and reinforced concrete plates [4] in combination with efficient convex optimization procedures.

On the other hand, assessing the ultimate load bearing capacity of constructions incorporating massive three-dimensional reinforced concrete components, which can no more be modelled as beams or plates, requires a specific analysis, such as the widely acknowledged “strut-and-tie” model (see among many other references [5], [6], [7] or [8]) which, in some way, can be related to the lower bound static approach of yield design. With a special attention to evaluating the ultimate shear capacity of reinforced concrete deep beams, both the lower and upper bound methods of yield design have been implemented in the context of a finite element formulation with the help of linear programming optimization techniques [9]. In this study, reinforced concrete was described according to a “*mixed modelling*” approach, in which plain concrete was modelled as a two-dimensional continuous medium under plane stress, while the reinforcement bars were treated as one dimensional flexible beams embedded in the concrete material.

The generalization to the more realistic situation of linear reinforcing inclusions placed into three-dimensional concrete bodies is posing a somewhat serious challenge as regards the possibility of treating such a case in a 1D-3D mixed modelling approach. Some attempts to circumvent this problem have already been proposed either in the context of the finite element formulation [10] or making use of an implicit homogenization method [11] or multiphase model [12].

The present contribution is devoted to applying the previously mentioned homogenization model, initially developed for reinforced soils, to the yield design of three-dimensional reinforced concrete structures. It is based on the combination of the following elements.

- Formulation of the plain concrete three-dimensional strength properties by means of a tension cut-off Mohr-Coulomb condition, characterized by the uniaxial tensile and compressive strengths of the concrete, along with its friction angle.
- Modelling the strength of each individual reinforcement with its surrounding concrete volume as a homogenized anisotropic continuum accounting for both the above mentioned plain concrete strength properties and axial strength of the reinforcing inclusion.

- Finite element formulation of the lower bound static approach of yield design based on a discretization of the structure into tetrahedral elements with a piecewise linear variation of the stresses.
- The final optimization procedure is carried out by means of Semi-definite Programming (SDP).

The whole design procedure is first illustrated and validated on the simple example of a uniformly loaded deep beam, and the obtained results are compared with those derived from a 1D modelling of the structure where the local resistance is defined by means of an interaction diagram. It is then applied to evaluating the ultimate bearing capacity of a reinforced concrete bridge pier cap subjected to concentrated vertical loads.

## 2. MODELLING STRENGTH PROPERTIES OF PLAIN AND REINFORCED CONCRETE

### 2.1. Plain concrete and reinforcing bars

Following the approach of [2] and [5] or quite recently [4], the unreinforced or plain concrete will be modelled as a 3D homogeneous continuous medium, the strength properties of which will be described by means of a *tension cut-off Mohr-Coulomb* yield condition which may be formulated as:

$$F^c(\underline{\sigma}) = \sup \{ K_p \sigma_M - \sigma_m - f_c; \sigma_M - f_t \} \leq 0 \quad (1)$$

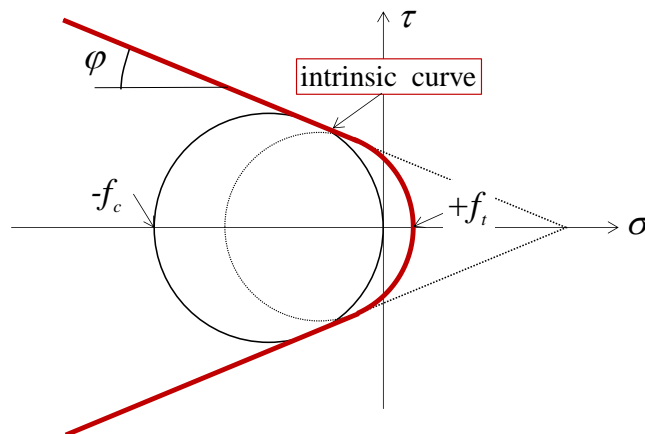


Figure 1. Geometrical representation of the tension-cut off Mohr-Coulomb criterion in the Mohr-plane

In the above condition,  $\sigma_M$  and  $\sigma_m$  represent the major and minor principal stresses, respectively (tensile stresses are counted positive throughout the text),  $f_t$  and  $f_c$  denote the *uniaxial* tensile and compressive resistances and  $K_p = (1 + \sin \varphi) / (1 - \sin \varphi)$  where  $\varphi$  is the internal friction angle which is usually taken equal to  $37^\circ$  ( $K_p \approx 4$ ). This criterion is thus defined by *three strength parameters*. It may for instance be represented by means of an intrinsic curve

in the Mohr-plane by as shown in Fig. 1, where the three material parameters defining the strength condition (1) are clearly apparent.

The concrete material is reinforced by one dimensional steel bars or rods, the strength condition of which may be expressed in terms of axial force  $n$  only, since their resistance to shear force  $v$  and bending moment  $m$  can be neglected:

$$-kn_0 \leq n \leq n_0, v = m = 0 \quad (2)$$

In the above condition,  $n_0$  denotes the tensile resistance of each individual reinforcing bar, while  $k$  is a non-dimensional parameter, ranging from 0 to 1, which accounts for a reduced resistance under compression, due to buckling for instance.

## 2.2. Reinforced concrete: a homogenized strength condition

Some significant regions of the reinforced concrete structure (such as deep beams: see for instance [2]) may be reinforced by such uniformly distributed bars (case of stirrups or open frames). Provided that the spacing between two neighbouring reinforcements is sufficiently small as compared with the size of the reinforced zone, the latter may be replaced by a zone where the homogenized constituent material obeys a macroscopic strength condition (see [13] for composite materials, or [14] for reinforced soils and [9] for reinforced concrete).

This macroscopic strength condition, which can be derived from using the yield design homogenization method [15], may be expressed as follows:

$$F^{rc}(\underline{\underline{\sigma}}) \leq 0 \Leftrightarrow \begin{cases} \underline{\underline{\sigma}} = \underline{\underline{\sigma}}^c + \sigma^r \underline{e}_1 \otimes \underline{e}_1 \\ \text{with } F^c(\underline{\underline{\sigma}}^c) \leq 0 \text{ and } -k\sigma_0 \leq \sigma^r \leq \sigma_0 \end{cases} \quad (3)$$

where  $\underline{e}_1$  is the unit vector parallel to the reinforcing bars, and  $\sigma_0$  is defined as the tensile resistance of these bars *per unit transverse area*:

$$\sigma_0 = n_0 / s^2 \quad (4)$$

where  $s$  is the spacing between the bars, which may also be expressed as:

$$\sigma_0 = A^s f_y^s / s^2 = \eta f_y^s \quad (5)$$

In the above equation,  $f_y^s$  denotes the uniaxial strength of the bar constituent material (steel) and  $A^s$  the bar cross-sectional area, so that  $\eta$  represents the *reinforcement volume fraction* (see Fig. 2(a) where  $s^2 = A^s + A^c$ ).

It is to be noted that the validity of the above macroscopic strength criterion (3) is subject to the verification of two important conditions (see [15] for more details):

- The reinforcing bars are perfectly bonded to the surrounding concrete material, which means for instance that no slippage occurs at the bar/concrete interface.

- The reinforcement volume fraction remains sufficiently small ( $\eta \ll 1$ ), whereas the resistance of the reinforcing material is much higher than that of the concrete material and notably its tensile strength ( $f_y^s \gg f_c$ ).

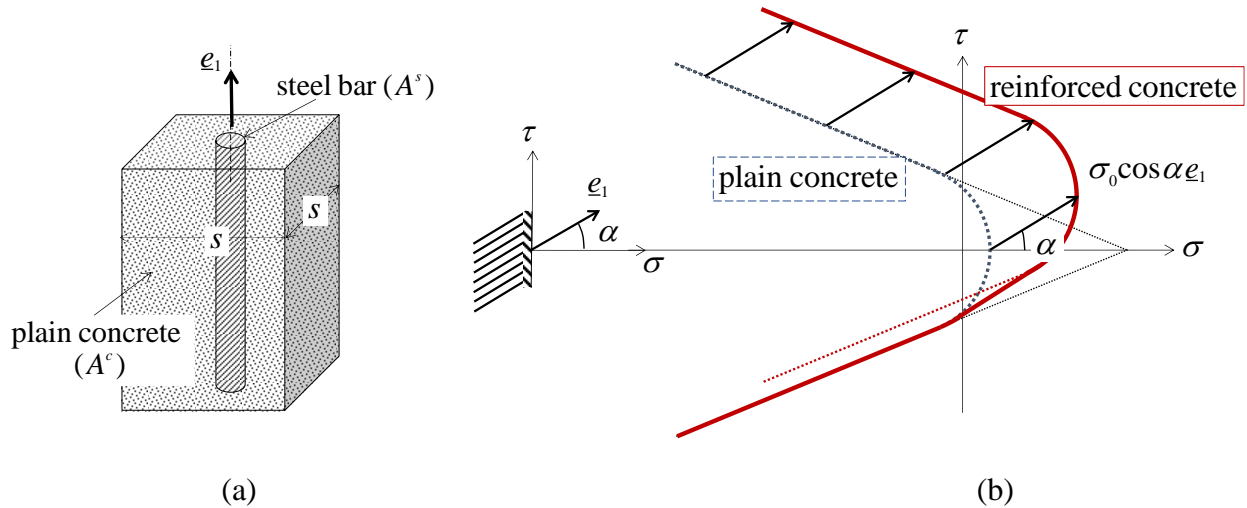


Figure 2. (a) Representative volume of reinforced concrete; (b) macroscopic strength condition relative to an oriented facet (case  $k=0$ )

Figure 2(b) illustrates the macroscopic strength condition (3) expressed on an oriented facet of the homogenized reinforced concrete in the particular case when  $k=0$  (no compressive resistance of the reinforcements). According to this figure, the corresponding strength domain in the  $(\sigma, \tau)$ -plane can be drawn simply as the convex envelope of the plain concrete intrinsic failure curve and of the curve derived from that one through a translation of vector  $\sigma_0 \cos \alpha e_1$ . Such a geometric representation thus gives a clear evidence of the *strength anisotropy* of the homogenized reinforced concrete in exactly the same way as for fibre composite materials.

It should be pointed out that, without any reference to the limit analysis or yield design homogenization theory, some authors [11] did make use of a strength criterion quite similar to (3), that is based on an intuitive additive decomposition of the total stress in reinforced concrete zones into stress components relating to the plain concrete and the reinforcements, each one complying with independently specified strength conditions.

### 2.3. The “mixed modelling” approach to reinforced concrete structures: a serious limitation

Referring now to the frequently encountered situation where only a small number of differently oriented reinforcements are incorporated in the concrete structure (case of longitudinal reinforcements in deep beams for instance), the above mentioned homogenization method is no more applicable and a so-called “mixed modelling” approach should be advocated. According to this approach, the reinforcements are treated as 1D structural elements with a strength condition defined by (2) embedded in the concrete material modelled as a 3D continuum, the strength of which is specified by (1).

Unfortunately, this 1D-3D mixed modelling approach comes against a serious limitation concerning the establishment of equilibrium equations for such a composite system. Indeed, the equilibrium equation at any point of the reinforcing bar may be written as:

$$\frac{dN(x_1)}{dx_1} + p(x_1) = 0 \quad (6)$$

where  $p$  represents the linear density of axial force exerted by the surrounding concrete material onto the reinforcing bar (Fig. 3(a)).

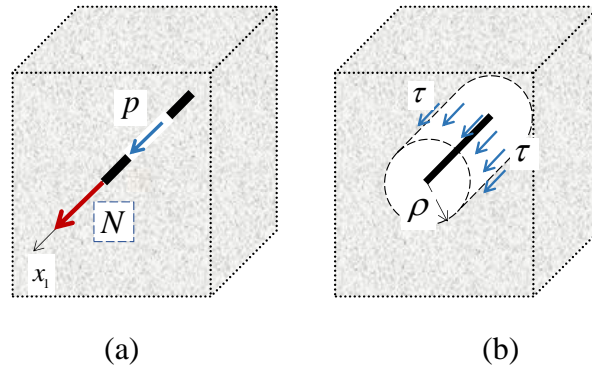


Figure 3. Interaction forces between concrete and reinforcement in the context of 1D-3D mixed modelling

Now, the impossibility of connecting such a 1D distribution  $p$  of interaction forces with the three-dimensional stress fields prevailing in the surrounding concrete material may be illustrated from the following simple reasoning. Considering a circular cylindrical “control surface” of radius  $\rho$  with its axis placed along the reinforcement, as shown in Fig. 3(b), the interaction force density  $p$  may be obtained from applying along this surface a longitudinal shear stress  $\tau$ , the average value of which along the circle drawn on this surface at point  $x_1$ , could be expressed as:

$$\langle \tau \rangle (x_1) = \frac{p(x_1)}{2\pi\rho} \quad (7)$$

According to the latter equation, the shear stress which should be developed in the concrete along the control surface for applying a given value of interaction force density  $p$  increases to infinity as the radius  $\rho$  tends to zero, so that the stress field in the concrete material would tend to infinity along the reinforcement axis. Such a singularity could possibly be taken into account in the context of a linear elastic behavior of the concrete, but definitely not as soon as yielding and failure of the latter is concerned, since in this case the yield strength condition (1) of the concrete would be systematically violated when approaching the 1D reinforcing bar.

#### 2.4. An extended homogenization-based model

Of course, the only fully mechanically consistent and rigorous way of circumventing the above limitation, would be to model each reinforcing bar as a three-dimensional volume body. But, on account of the small diameter of such bars along with the sharp contrast between the reinforcing steel and the surrounding concrete in terms of strength properties, this would

undoubtedly imply prohibitive computational costs, due for instance to the highly refined discretization required when employing finite element techniques.

An alternative approach for the finite element modelling of 1D steel inclusions in 3D concrete volumes has been recently proposed by [10]. Likewise, in a more explicit reference to the homogenization procedure, three dimensional fem elastoplastic analyses on reinforced concrete structural elements have been performed by [12]. Their approach, which will be adopted in this contribution, may be described as follows.

Considering one individual 1D-inclusion embedded in a 3D-concrete block, a cylindrical volume of concrete with the inclusion placed along its axis is defined, as shown in Fig. 4(a). The intuitive idea is to replace the composite cylindrical volume, thus obtained, by a homogenized cylinder, at any point of which the strength condition is defined by Eqs. (3) and (4), where  $s$  represents the side of the squared cross-section of the cylindrical volume.

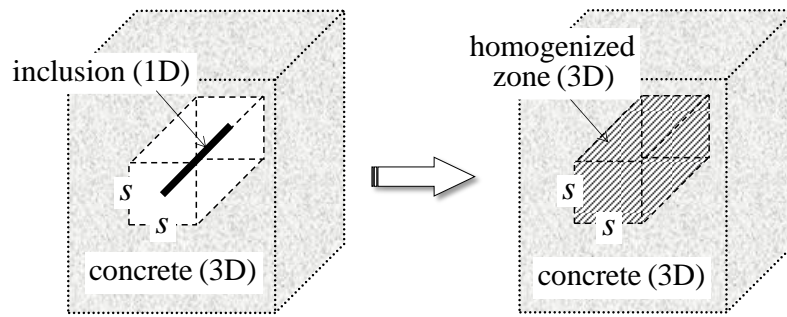


Figure 4. Construction of a homogenized reinforced zone around an individual inclusion

The advantage of such a modelling procedure, is that the characteristic size of the homogenized zone (namely  $s$ ) is significantly larger than the inclusion's diameter, thus allowing for example a much easier finite element discretization of the reinforced concrete structure as a 3D-3D composite, since a refinement of the mesh around the inclusion is no more required for obtaining accurate and reliable predictions. Of course, the choice of  $s$  being arbitrary, it will be necessary to make sure that the results of the computations performed on the basis of this model, remain rather insensitive to the value of  $s$ .

### 3. NUMERICAL IMPLEMENTATION OF THE LOWER BOUND STATIC APPROACH

#### 3.1. Statement of the yield design problem

Assuming that the reinforced concrete structure under consideration is subject to one single loading parameter  $Q$ , the ultimate or failure load value  $Q^+$  is defined, in the context of the yield design theory, as the maximum value of  $Q$  for which one can exhibit any stress field  $\underline{\sigma}$  :

- ✓ *statically admissible* (S.A.) with  $Q$ , i.e. verifying the equilibrium equation at any point of the structure:

$$\operatorname{div}\underline{\sigma}(x) + \rho E(x) = 0, \forall x \in V \quad (8)$$

where  $\rho \underline{F}$  denotes the body force volume density (material specific weight for example), along with the continuity of the stress-vector across possible stress jump surfaces  $\Sigma$ :

$$[\underline{\sigma}(\underline{x})] \cdot \underline{n}(\underline{x}) = 0, \quad \forall \underline{x} \in \Sigma \quad (9)$$

as well as the stress boundary conditions associated with the loading  $Q$ ;

- ✓ while complying with the strength conditions assigned to the plain concrete and reinforced concrete zones of the structure, respectively:

$$F^c(\underline{\sigma}(\underline{x})) \leq 0 \quad \forall \underline{x} \in V^c \quad \text{and} \quad F^{rc}(\underline{\sigma}(\underline{x})) \leq 0 \quad \forall \underline{x} \in V^{rc}, \quad V = V^c \cup V^{rc} \quad (10)$$

where  $V^c$  (respectively  $V^{rc}$ ) represents the part of the structure occupied by the plain concrete (resp. by the homogenized reinforced concrete).

### 3.2. 3D finite element discretization

Applying the lower bound static approach consists in considering S.A. stress fields depending either on a small number of parameters in an analytical approach, or on a large but finite number of stress variables in a numerical approach, such as the finite element method. According to the latter, the geometrical domain  $V$  occupied by the three-dimensional structure is discretized into  $N_e$  tetrahedral finite element  $V^e$ , such as the one depicted in Fig. 5(a), with a linear variation of the stress field inside each element so that the stress at any point inside such an element may be classically written as:

$$\forall \underline{x} \in V^e, \quad \underline{\sigma}(\underline{x}) = \sum_{k=1}^4 N^k(\underline{x}) \underline{\sigma}^k \quad (11)$$

where  $N^k$ ,  $k=1$  to 4, are four linear interpolation functions and  $\underline{\sigma}^k$  is the value of the stress tensor at the node  $n^{\circ k}$  of the element. It is to be noted that there are as many stress tensors  $\underline{\sigma}^k$  attached to any geometrical node of the mesh as there are tetrahedral elements sharing this node as an apex.

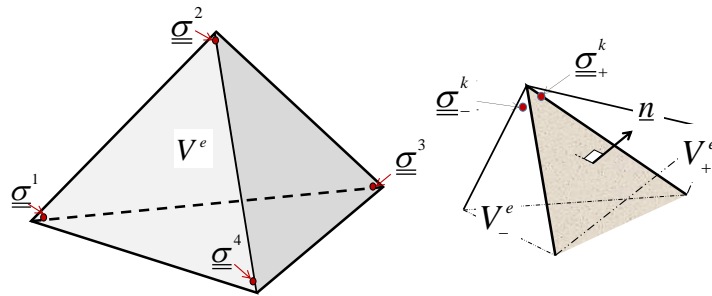


Figure 5. Four noded tetrahedral finite element used in the discretization of the reinforced concrete structure

Furthermore, one may come across two situations.

- ✓ The considered element is located in the unreinforced plain concrete zone  $V^c$  of the structure, so that the stress state at any node of this element is defined by one single tensor which should comply with the strength condition (1).

- ✓ The element is located in the homogenized reinforced concrete zone  $V^c$  and, as suggested by the corresponding homogenized strength condition (3), the stress state is defined by a stress tensor and an additional scalar stress variable which must satisfy separate independent strength conditions.

It follows that a total of, either  $4 \times 6 = 25$  or  $4 \times 7 = 28$  stress variables, is attached to each element  $V^e$  of the mesh.

### 3.3. Formulation of equilibrium conditions as linear constraints on the stress variables

On account of (11), the equilibrium equation (8) inside each element may be rewritten as:

$$\forall \underline{x} \in V^e, \text{div} \underline{\underline{\sigma}}(\underline{x}) = \sum_{k=1}^4 \underline{\text{grad}} N^k \cdot \underline{\underline{\sigma}}^k = -\rho \underline{F} \quad (12)$$

where it is assumed that the body force density is constant over the element. Since the gradient of each interpolation function is constant, Eq. (11) represents a *linear constraint* on the nodal stress variables  $\underline{\underline{\sigma}}^k$  of each element. It is worth noting that the linear equilibrium condition (11) involves the *total* stress in the homogenized reinforced concrete and not the “partial” stresses  $\underline{\underline{\sigma}}^c$  and  $\sigma^r$  which appear in the definition (3) of the reinforced concrete strength condition.

Likewise, Eq. (8) expresses the continuity of the (total) stress vector across any triangular facet common to two adjacent elements (see Fig. 5(b)). It also leads to linear constraints of the form:

$$(\underline{\underline{\sigma}}_+^k - \underline{\underline{\sigma}}_-^k) \cdot \underline{n} = 0 \quad (13)$$

where  $\underline{n}$  is the unit normal to the triangular facet connecting two such adjacent elements  $V_+^e$  and  $V_-^e$ . Owing to the linear variation of the stress fields and to the convexity of the strength conditions, checking the jump condition (13) at the nodal points is sufficient to make sure that it is verified at any point of the discontinuity triangular facet.

It follows that all the conditions that a discretized stress field must satisfy for being statically admissible with a load value  $Q$  may be formulated in a generic matrix form as:

$$\underline{\underline{\sigma}}^{\text{fem}} \text{ S.A. with } Q \Leftrightarrow \begin{cases} Q = {}^T \{A\} \{\Sigma\} \\ \text{with } [B] \{\Sigma\} = \{C\} \end{cases} \quad (14)$$

where  $\{\Sigma\}$  is a column-vector which collects all the nodal stress variables associated with the mesh discretization of the structure, that is the total stresses in the plain concrete zones and the partial stresses in the homogenized reinforced parts.

Consequently, the finite element implementation of the lower bound static approach of yield design reduces to the following *maximisation problem*:

$$Q^+ \geq Q^{lb} = \text{Max}_{\{\Sigma\}} Q = {}^T \{A\} \{\Sigma\} \text{ subject to } \begin{cases} [B] \{\Sigma\} = \{C\} & \text{equilibrium} \\ F(\{\Sigma\}) \leq 0 & \text{strength criteria} \end{cases} \quad (15)$$

where  $F(\{\Sigma\}) \leq 0$  represents the conditions expressing the different *strength criteria* to be satisfied. Again, due to the linear variations (11) of the considered stress fields and to the *convexity* of the strength conditions, the latter have only to be verified at the nodal stress points.

### 3.4. Formulation as a SDP problem

Unlike the equilibrium conditions which involve the total stresses only, the strength criteria in the homogenized reinforced zones concern the partial stresses as shown by (3). While the condition relating to the reinforcement writes in the form of a simple *linear* constraints ( $-k\sigma_0 \leq \sigma' \leq \sigma_0$ ), the strength condition of the plain concrete defined by (1) involves the maximal and minimal principal stress components. The latter thus needs a specific treatment so that the optimization problem (15) may be treated as a *Semi-definite programming* (SDP) optimization problem [16] as briefly explained below.

*Semi-definite Programming* (SDP) allows to formulate optimization problems in terms of constraints on eigenvalues of symmetric matrices. It therefore provides a suitable framework for the tension cut-off Mohr-Coulomb criterion (1) which involves the maximal and minimal principal stress components (eigenvalues). Thus, the three-dimensional Mohr-Coulomb criterion can be enforced by applying the two following *linear matrix inequalities* (LMI):

$$t_M \underline{\underline{1}} - \underline{\underline{\sigma}} \succeq 0 \quad \text{and} \quad t_m \underline{\underline{1}} - \underline{\underline{\sigma}} \preceq 0^1 \quad (16)$$

in conjunction with the equality constraint:

$$K_p t_M - t_m - f_c = 0 \quad (17)$$

where  $t_M$  and  $t_m$  are auxiliary variables. Eliminating  $t_M$  from Eq. (17) yields:

$$\underline{\underline{\sigma}} - K_p^{-1} t_m \underline{\underline{1}} \preceq K_p^{-1} f_c \underline{\underline{1}} \quad \text{and} \quad t_m \underline{\underline{1}} - \underline{\underline{\sigma}} \preceq 0 \quad (18)$$

The second inequality of (18) can be expressed as:

$$t_m \underline{\underline{1}} - \underline{\underline{\sigma}} + \underline{\underline{X}} = 0 \quad \text{and} \quad \underline{\underline{X}} \succeq 0 \quad (19)$$

which allows the stress variable to be eliminated using the relationship:

$$\underline{\underline{\sigma}} = t_m \underline{\underline{1}} + \underline{\underline{X}} \quad (20)$$

so that the first inequality of (18) becomes:

$$\underline{\underline{X}} + (1 - K_p^{-1}) t_m \underline{\underline{1}} \preceq K_p^{-1} f_c \underline{\underline{1}} \quad (21)$$

or introducing  $\underline{\underline{Y}}$  as a second auxiliary symmetric matrix variable, the three dimensional Mohr-Coulomb strength criterion may finally be reformulated as:

$$\begin{aligned} \underline{\underline{X}} + \underline{\underline{Y}} + (1 - K_p^{-1}) t_m \underline{\underline{1}} &= K_p^{-1} f_c \underline{\underline{1}} \\ \text{with } \underline{\underline{X}} \succeq 0 \quad \text{and} \quad \underline{\underline{Y}} \succeq 0 \end{aligned} \quad (22)$$

which lends itself very easily to the numerical treatment by a SDP solver such as [17].

---

<sup>1</sup> where  $\underline{\underline{A}} \succeq 0 \Leftrightarrow x \underline{\underline{A}} x \geq 0 \quad \forall x$

Similarly, the Rankine-type cut-off strength criterion which limits the tensile stresses in the plain concrete material:

$$\sigma_M - f_t \leq 0 \Leftrightarrow \underline{\underline{\sigma}} - f_t \underline{\underline{1}} \leq 0 \quad (22)$$

may be recast into the following constraints:

$$\underline{\underline{\sigma}} + \underline{\underline{Z}} + f_t \underline{\underline{1}} = 0 \quad \text{and} \quad \underline{\underline{Z}} \succeq 0 \quad (23)$$

where a third auxiliary symmetric matrix variable  $\underline{\underline{Z}}$  has been introduced.

## 4. A FIRST ILLUSTRATIVE TEST EXAMPLE

### 4.1. Problem description

A specific computer code implementing the whole above described numerical procedure, has been devised for calculating numerically optimized *lower bounds* to the ultimate loads of three dimensional reinforced concrete structures. A first illustrative application of this code is performed on the illustrative example of a beam of length  $L$  varying between 0,5 m and 16m and rectangular cross-section ( $H=0.5$  m,  $b=0.2$  m), subject to a uniform *surface loading*  $q$  applied onto the top of the beam (Fig. 6). The left end ( $X=0$ ) of the beam is perfectly *clamped* (velocity vector equal to zero:  $\underline{U}=0$ ), while the boundary conditions at the right end ( $X=L$ ) are:

$$T_x = \sigma_{xx} = 0, \quad U_y = U_z \quad (24)$$

which, in the framework of a 1D model of the beam, corresponds to a simple support free to move horizontally along the  $X$ -axis and rotate about the  $Y$ -axis (axial force  $N$  and bending moment  $M$  are set equal to zero).

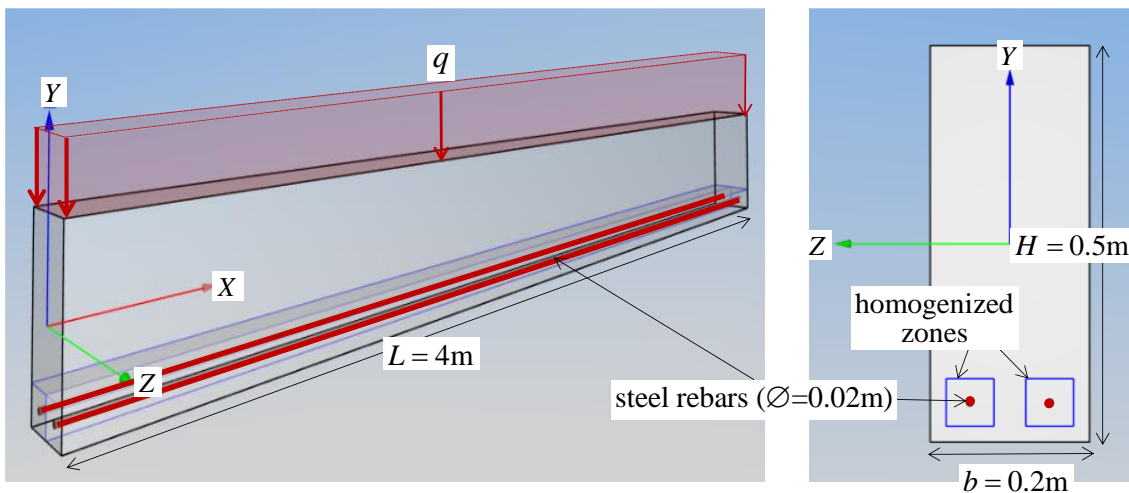


Figure 6. Reinforced concrete beam of length under uniform loading (case  $L=4\text{m}$ ).

The beam is made of a homogeneous concrete material, with the following uniaxial tensile and compressive strength characteristics:

$$f_t = 0.5 \text{ MPa} \quad \text{and} \quad f_c = 40 \text{ MPa} \quad (25)$$

keeping in mind that, referring to a tension cut-off Mohr-Coulomb condition, the value internal friction angle  $\varphi$  is taken equal to  $37^\circ$ .

The beam is reinforced by two longitudinal rebars of diameter equal to 2cm, made of a steel with a uniaxial strength equal to  $f_y^s=400$  MPa. The bars are placed at the bottom part of the beam cross section as shown in Fig.5. Two methods will now be employed to evaluate the ultimate load  $q^+$  of this simple structure.

#### 4.2. Modelling the structure as a 1D beam

The structure is first schematized as a 1D beam subjected to a uniform loading of linear density  $qb$ , so that the statically admissible distribution of axial force and bending moment is of the form (Fig. 7):

$$N = 0, M(X) = R(L - X) - \frac{qb}{2}(L - X)^2 \quad (26)$$

where  $R$  is the unknown reaction at the right hand simply supported end ( $X=L$ ).

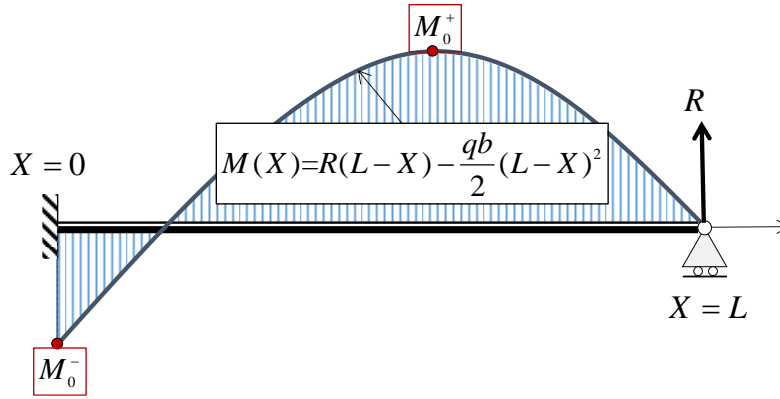


Figure 7. Statically admissible bending moment distribution in the structure modelled as a 1D-beam

It may be classically shown that the exact limit load of this structure is obtained when the corresponding bending moment parabolic distribution is such that (see Fig. 7):

$$M(X=0) = M_0^-, \text{Max}\{M(X), 0 \leq X \leq L\} = M_0^+ \quad (26)$$

where  $M_0^+$  (respectively  $M_0^-$ ) is the strength of the beam under pure (that is for  $N=0$ ) positive (resp. negative) bending. This leads to the following expression for limit load:

$$q_{\text{ld}}^+ = \frac{2}{bL^2} \left[ 2M_0^+ - M_0^- + 2\sqrt{M_0^+(M_0^+ - M_0^-)} \right] \quad (27)$$

The actual values of  $M_0^\pm$  may be obtained from the *interaction diagram of the reinforced concrete beam section*, the geometrical and strength characteristics of which are shown in Fig. 8. More precisely, the *interaction domain*  $G^c$  of the plain concrete section being defined as:

$$(N, M) \in G^c \Leftrightarrow |M| \leq \frac{H}{2} \frac{(N + N_c)(N_t - N)}{(N_t + N_c)^2} \quad (28)$$

for  $-bHf_c = -N_c \leq N \leq N_t = bHf_t$

the reinforced section interaction domain  $G^{rc}$  is defined as (see [18] and [19] for more details concerning the yield design–based procedure used for determining such interaction domains):

$$G^{rc} = \{G^c + \lambda(1, \delta); -2kn_0 \leq \lambda \leq 2n_0\} \quad \text{with } n_0 = (\pi\varnothing^2 / 4)f_y^s \quad (29)$$

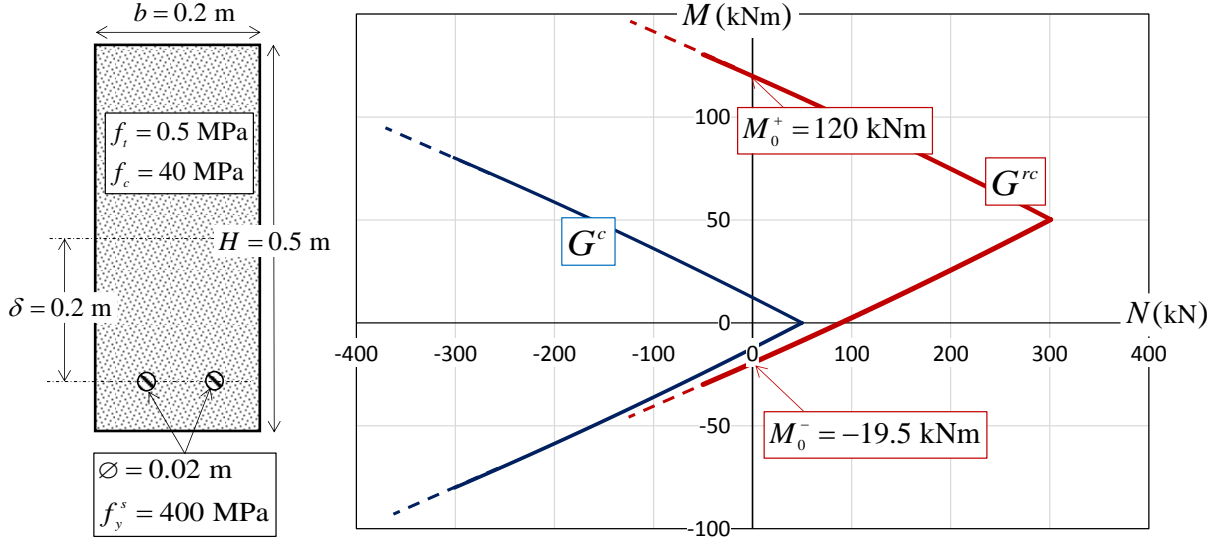


Figure 8. Interaction domains of plain concrete and reinforced concrete sections in the  $(N, M)$ -plane.

Both domains have been represented in Fig. 8 for the set of selected values recalled in the same figure. The values of the resistance of the reinforced concrete section under pure bending correspond to the intersecting points of the boundary line of  $G^{rc}$  with the  $M$ -axis:

$$\begin{aligned} M_0^+ &= \text{Max} \{M; (N=0, M) \in G^{rc}\} \cong 120 \text{ kNm} \\ M_0^- &= \text{Min} \{M; (N=0, M) \in G^{rc}\} \cong -19,5 \text{ kNm} \end{aligned} \quad (30)$$

Hence the final expression of the limit load as a function of the beam length  $L$ :

$$q_{\text{ld}}^+ (\text{MPa}) \cong \frac{5.18}{L^2} \quad (31)$$

#### 4.3. 3D-modelling of the structure:

The structure is now treated as a three dimensional parallelepipedic volume. According to the method described in section 2.4, each bar with its surrounding volume of concrete material is replaced by a homogenized material obeying the macroscopic strength condition (3) with:

$$\sigma_0 = \frac{n_0}{s^2} = \frac{\pi\varnothing^2 f_y^s}{s^2} \quad (32)$$

where  $s^2$  is the cross section area of the homogenized volume.

First, several numerical analyses using the dedicated SDP optimization procedure described earlier are performed for the  $L=4\text{m}$  long reinforced concrete beam with different homogenized volume cross sections  $s^2$ . The purpose of this study is to validate the proposed method, and notably the homogenization procedure. The results will then be compared to the 1D beam calculation developed in section 4.3.

As previously explained in section 2.4, the homogenized method consists in replacing each individual rebar by a larger surrounding volume with adapted macroscopic strength condition, thereby allowing to perform numerical analyses without the computational cost induced by a much refined meshing of each rebar. Thus, both bottom longitudinal rebars being replaced by such homogenized volumes, three cases with different homogenized volume cross sections, namely  $s^2=(b/2)^2=0.1\times 0.1\text{ m}^2$ ,  $s^2=0.08\times 0.08\text{ m}^2$  and  $s^2=0.06\times 0.06\text{ m}^2$  (configuration of Fig. 6) have been investigated.

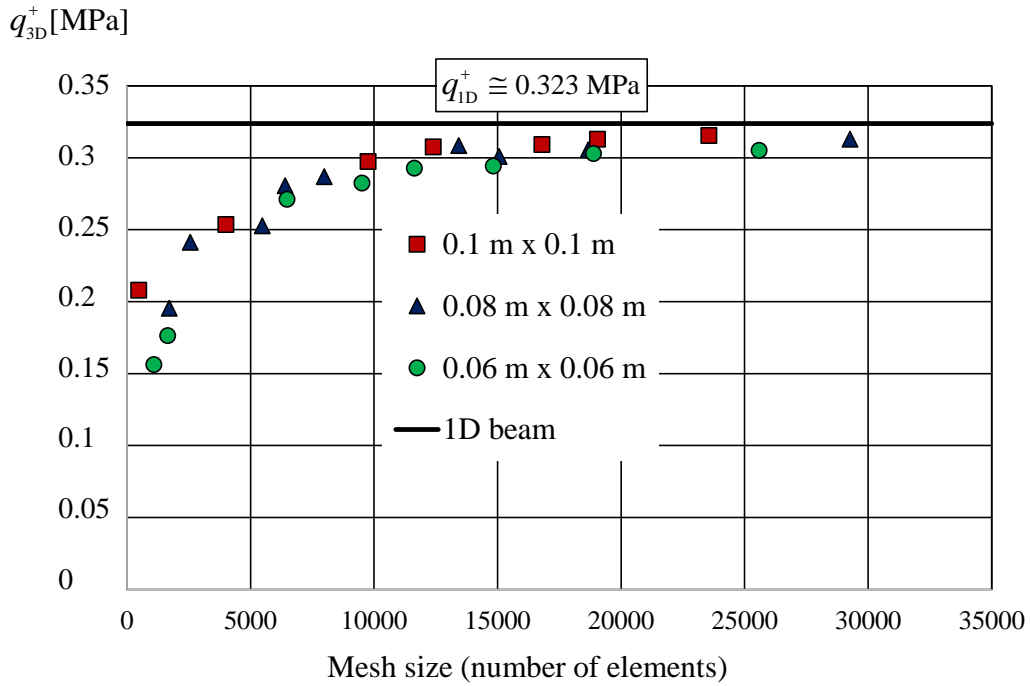


Figure 9. Lower bound estimate of the beam ultimate bearing capacity as a function of the mesh size, for three different homogenized volume cross sections ( $L=4\text{m}$ )

The results have been reported in Fig. 9 which shows the variations of the lower bound estimate for the ultimate load bearing capacity of the reinforced concrete beam ( $q_{3D}^+$ ) as a function of the mesh size (number of elements), for each of the three cases. The result of the 1D-beam calculation performed in section 4.2 is also plotted in the same figure in the form of a horizontal straight line.

The following comments can be made.

- ✓ For each of the three configurations, several finite element analyses have been performed where the number of finite elements has been increased from a few hundreds to about

30 000. Figure 9 clearly shows that the corresponding lower bound estimate is also increasing with a stabilization as soon as the mesh size exceeds 10 000 elements.

- ✓ The results presented here clearly assess the validity of the proposed homogenization method for treating the case of a reinforcement by few individual inclusions. Indeed, the results of the evaluation of the ultimate load bearing capacity for the three cases are almost insensitive to the size of the proposed homogenized volume cross sections.
- ✓ Finally, even if it should be kept in mind that the obtained results are lower bound estimates for the exact ultimate bearing capacity of the beam, the strengthening effect due to the presence of the rebars in the concrete beam is strikingly apparent, since the evaluation of the ultimate failure load, equal to 40kPa for the plain concrete beam of length  $L=4m$ , is increased to more than 300kPa when the reinforcement by two longitudinal bars is taken into account.

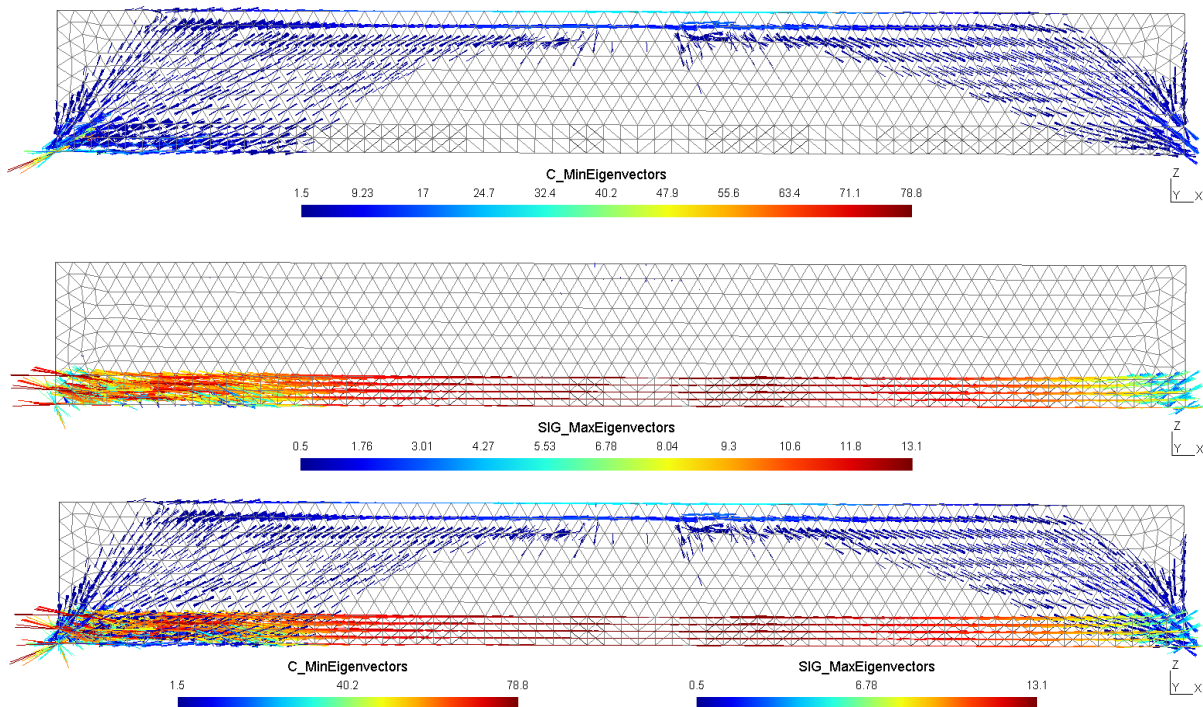


Figure 10. Longitudinal views of the optimized stress field in the plain concrete (top picture), reinforced zones (intermediate picture) and entire structure (bottom picture) for  $L=4m$

Figure 9 provides longitudinal views of the optimized stress field in the case where  $s^2=0.1 \times 0.1 \text{ m}^2$ . The top figure shows the distribution of the principal compressive stresses prevailing in the plain concrete material, while the intermediate figure represents the principal tensile stresses mobilized in the homogenized reinforced zones. Both distributions are superimposed in the bottom figure. Calculations were performed on an INTEL XEON CPU E5-2673 @2.3 GHz CORE in about 373 seconds (six minutes) for the most refined mesh (23352 tetrahedrae). This underlines the decisive advantage of the proposed homogenization method over a direct approach where the inclusions should have been very finely discretized in and around the inclusions, which may lead to an oversized numerical problem. Moreover, it is worth pointing

out that a little less performing lower bound estimate for the ultimate load bearing capacity of the structure may be obtained (307kPa vs 315kPa) with a coarser mesh (composed of 12392 elements), leading to a computational time of 171 seconds.

	$L=16$ m	$L=8$ m	$L=4$ m	$L=2$ m	$L=1$ m
$q_{1D}^+$ (MPa)	0.0202	0.081	0.323	1.295	5.18
$q_{3D}^+$ (MPa)	0.0195	0.0794	0.3155	1.260	4.22
$\Delta$	+3.6%	+2%	+2.3%	+2.8%	+22.8%

Table 1. Comparison between  $q_{3D}^+$  and  $q_{1D}^+$  for different beam lengths

In order to compare the results derived from the 1D and 3D modellings of the structure, the effect of the length of the beam on its ultimate bearing capacity is now examined, all the other characteristics being kept unchanged. Several numerical analyses have been run to this end for different beam lengths (with  $s^2=0.01$  m<sup>2</sup>). The corresponding results are presented in Table 1. It appears that both evaluations are in excellent agreement for  $L \geq 2$ m, the 3D evaluation being slightly lower than the 1D calculation, which seems to be consistent with the fact that the 3D approach is a lower bound estimate.

On the other hand, as could be expected, both estimates are diverging for shorter beams, the 3D estimate being for instance 22.8% lower than the 1D calculation for  $L=1$ m. Of course, this discrepancy should be attributed to the fact that the 1D modelling is only applicable to sufficiently slender structures and not to “short” or “deep” beams where a limited shear resistance of the beam should be taken into account, which is implicitly made in the 3D calculation.

## 5. A PRACTICAL CASE STUDY: FAILURE DESIGN OF A BRIDGE PIER CAP

In order to assess the performance of the yield design numerical tool in situations where truly massive three dimensional structures are concerned, the following representative design case is now examined: a  $3 \times 3 \times 1.5$  m<sup>3</sup> parallelepiped concrete block is considered as a simplified model of bridge pier cap. The finite element lower bound static approach is performed on this structure subject to four vertical loads representing the action of the overlying bridge deck, as shown in Fig. 11. These loadings are applied in the form of a uniform pressure applied on top of small rigid square pads of  $0.7 \times 0.7$  m<sup>2</sup>. The interaction with the underlying bridge pier is modelled by imposing a rigid connection on a  $1.5 \times 0.7$  m<sup>2</sup> rectangular area placed at the centre of the bottom surface.

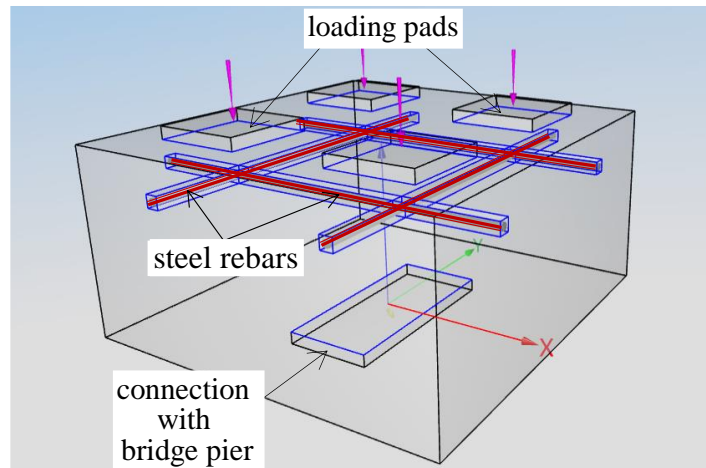


Figure 11. Reinforced concrete pier cap subject to bridge deck loading

The concrete block is made of a homogeneous plain concrete material, with  $f_c = 40\text{MPa}$  and  $f_t = 0.5\text{MPa}$ . It is strengthened by four steel rebars of diameter equal to 3cm, placed just below the loading pads as shown in Fig. 11, with a uniaxial strength equal to  $f_y^s = 400\text{MPa}$ . According to the above described procedure, each of the four rebars is replaced by a homogenized volume of square cross section equal to  $s^2=0.01\text{ m}^2$ .

The whole structure being discretized into 41904 tetrahedral finite elements, an optimal lower bound estimate for its ultimate load bearing capacity has been obtained using the SDP maximization procedure. Fig. 12 represents the distribution of the principal compressive stresses prevailing in the plain concrete material, while the principal tensile stresses mobilized in the (homogenized) reinforced zones are shown in Fig. 13. Both distributions have been superimposed in Fig. 14 which displays a perspective and a front views. Calculations were performed on the same computational server in approximately 1782 seconds (half an hour).

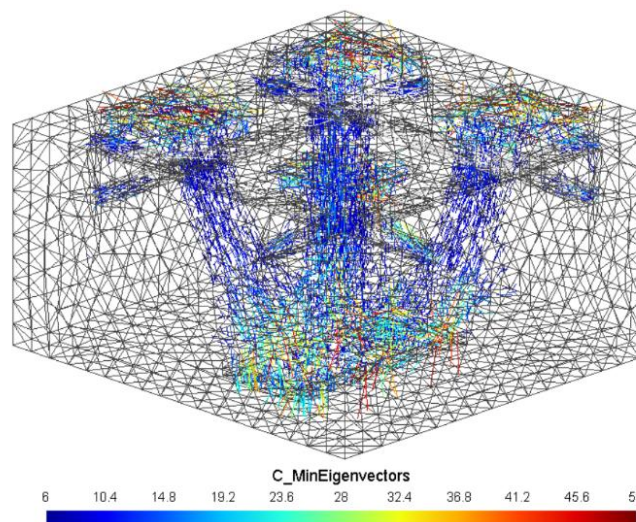


Figure 12. Perspective view of the optimized stress field in the concrete (compressions)

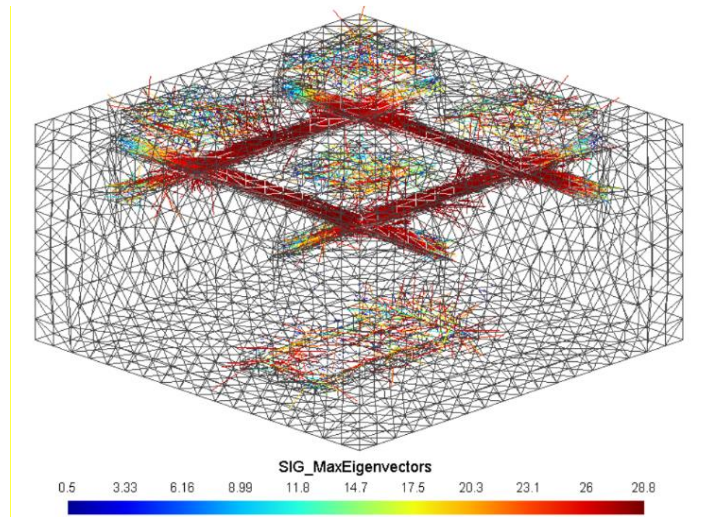


Figure 13. Optimized stress field in the homogenized zones (tractions)

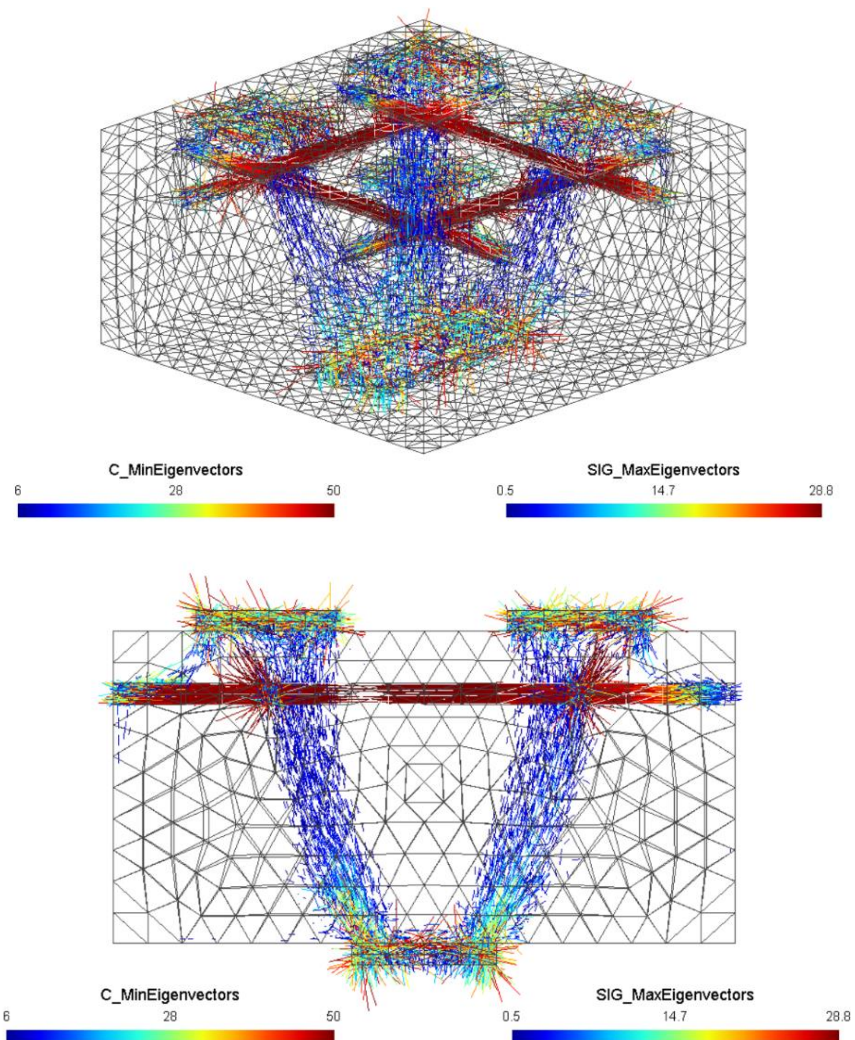


Figure 14. Perspective and front views of the optimized stress field in the whole pier cap

The thus obtained lower bound estimate for the ultimate bearing capacity of the reinforced concrete structure is equal to 4.69 MPa applied on each of the four loading pads. By way of comparison, the lower bound evaluation of the ultimate bearing capacity of the same non-reinforced concrete structure is equal to 3.18MPa. This means that the presence of the reinforcements increases the global resistance of the pier cap by as much as 47%.

The proposed model of three-dimensional reinforced concrete structures advocated in this contribution, as well as the feasibility of the related numerical approach in the context of the finite element method, have thus been successfully tested here on a representative example of massive reinforced concrete structure. The front view of Fig. 14 in particular, gives a clear intuition of the optimized stress field equilibrating the applied loading, exhibiting compressive stresses (*struts*) in the concrete material and tensile stresses in the homogenized reinforced zones (*ties*).

## 6. CONCLUSION

A specifically dedicated finite element computer code has been set up aimed at producing rigorous lower bound (*i.e.* conservative) estimates for the ultimate load bearing capacity of three-dimensional reinforced concrete structures in the context of the yield design approach. It relies upon two recent decisive breakthroughs: the numerical formulation of the corresponding optimization problem using efficient SDP optimization techniques, on the one hand, the adoption of a homogenization-inspired model for describing the mechanical behaviour of individual reinforcing inclusions embedded in a surrounding three-dimensional concrete matrix, on the other hand. The procedure may be further extended on two important points.

- The development of the same kind of numerical method and related computer tool in the framework of the yield design kinematic approach, which will provide upper bound estimates. Comparing the latter with the already determined lower bound estimates, will considerably help improve the accuracy and reliability of the design procedure.
- The adoption of a *multiphase model*, which may be perceived as an extension of the homogenization method [15], making it possible to take a specific interaction failure condition between the reinforcements and the concrete material, into account.

## REFERENCES

- [1] Salençon J. (2013) *Yield Design*, ISTE Ltd, Wiley, London.
- [2] Chen W.F. (1982) *Plasticity in reinforced concrete*, McGraw-Hill, New-York.
- [3] Bleyer J., de Buhan P. (2013). Yield surface approximation for lower and upper bound yield design of 3D composite frame structures, *Computers and Structures*, 129, pp. 86-98.
- [4] Bleyer J., Pham D.T., de Buhan P. (2015). Failure design of high-rise concrete panels under fire loading, *Engineering and Computational Mechanics*, Volume 168 Issue EM4, pp. 178-185.
- [5] Marti P. (1985). Truss models in detailing, *Concr. Int.*, 7(12), pp. 66-73.
- [6] Schlaich M., Schäfer K., Jennewein M. (1987). Toward a consistent design of structural concrete, *PCI Jl.*, 32(3), pp. 74-150.
- [7] Schlaich M., Anagnostou G. (1990). Stress Fields for Nodes of Strut-and-Tie Models, *Jl. of Structural Engineering*, Volume 126, N°1, pp. 13-23.
- [8] Siao W. B. (1993). Strut-and-tie model for shear behaviour in deep beams and pike caps failing in diagonal splitting, *ACI Struct. J.*, 90(4), pp. 356-363.
- [9] Averbuch D., de Buhan P. (1999). Shear Design of Reinforced Concrete Deep Beams: A Numerical Approach, *Jl. of Structural Engineering*, Volume 125, N°3, pp. 309-318.
- [10] Llau A., Jason L., Dufour, F., Baroth J. (2016). Finite element modelling of 1D steel components in reinforced and pre-stressed concrete structures, *Engineering Structures*, 127, pp. 769-783.
- [11] Nielsen M.P., Hoang L.C. (2010). *Limit Analysis and Concrete Plasticity*, CRC Press, Taylor & Francis.
- [12] Figueiredo M.P., Maghous S., Filho A.C. (2013). Three-dimensional finite element analysis of reinforced concrete structural elements regarded as elastoplastic multiphase media, *Materials and Structures*, 46, pp. 383-404.
- [13] de Buhan P., Taliercio A. (1991). A homogenization approach to the yield strength of composite materials, *European Journal of Mechanics, A/Solids*, 10, n°2, pp. 129-150.
- [14] Michalowski P.V., Zhao A. (1996). Failure of fiber-reinforced granular soils, *Jl. Geotech. Eng.*, ASCE, 122(3), pp. 226-234.
- [15] de Buhan P., Bleyer J., Hassen G. (2017). *Elastic, Plastic and Yield Design of Reinforced Structures*, ISTE-Elsevier, London.

- [16] Martin C.M., Makrodimopoulos A. (2008). Finite–Element Limit Analysis of Mohr–Coulomb Materials in 3D Using Semidefinite Programming, *Jl. Eng Mech.*, ASCE, Vol. 134, N°4, pp. 339-347.
- [17] The Mosek optimization software: available from <http://www.mosek.com>
- [18] Averbuch D. (1996) *A yield design-based approach to reinforced concrete structures*, PhD thesis, ENPC, Paris (in French).
- [19] Pham D.T., de Buhan P., Florence C., Heck J.-V., Nguyen H. N. (2015) Interaction diagrams of reinforced concrete sections in fire: a yield design approach, *Eng. Struct.* 90, pp. 38-47.